Dependence of Operation Density on the Density Profile Shape in DEMO Plasmas with Ar Injection for Divertor Heat Load Reduction

Ryosuke SAKAI, Takaaki FUJITA and Atsushi OKAMOTO

Nagoya University, Furo-cho, Chikusa-ku, Nagoya 464-8603, Japan

(Received 17 July 2019 / Accepted 1 April 2020)

The feasibility of operation with high plasma density assumed in DEMO conceptual designs is one of the major concerns. Although the operation density would be reduced if peaked density profiles are realized, accumulation of impurity ions injected for divertor heat load reduction may be a problem. We analyzed the argon (Ar) ion transport in the core plasma with various density profile shapes, under the condition of the given fusion power maintained by the feedback control of injection frequency of deuterium-tritium pellets, using the TOTAL code. The ratio of the Ar density to the electron density was fixed at 0.5%, the expected value in JA DEMO, on the plasma surface. For the peaked density profiles, Ar was accumulated in the central region, which caused larger increment in the electron density, but the increment was smaller than the reduction of operation density by peaking the fuel density profile in moderately peaked cases. As a result, the line-averaged electron density and the pedestal electron density were in the feasible ranges reported in the previous experimental study, for moderately peaked density profiles. It was revealed that making the peaked density profiles can improve the feasibility of the DEMO operation density.

Keywords: operation density, density profile, impurity transport, DEMO, radiation loss

DOI: 10.1585/pfr.15.1303031

In most of conceptual design studies of DEMO and fusion power plants, including JA DEMO 2014 [1], high operation plasma density, larger than the Greenwald limit, is assumed and then its feasibility is one of major concerns. It is known that the same fusion power can be obtained with lower volume-averaged density and lower peripheral density for centrally peaked density profiles. Prediction of density profile is, however, difficult since the turbulent convection is not negligible compared to the turbulent diffusion in the particle transport. The dependence of the turbulent convection on the local plasma parameters can change significantly and even the direction can be either in the inward direction (pinch) and in the outer direction [2]. Furthermore, the effects of the turbulent convection are enhanced and our prediction capability would be more limited for DEMO and fusion power plants since the fuel supply in the central region is negligibly small in these devices. Therefore it is needed to investigate the dependence of the fusion performance and the required operation parameters on density profile shapes in conceptual design studies of DEMO and fusion power plants.

For DEMO and the fusion power plant, injection of impurity such as argon (Ar) in the divertor region is planned as a candidate in order to reduce the heat load to divertor target, while its accumulation in the core plasma is concerned. The impurity accumulation leads to fuel dilution and increased radiation from the core plasma, both of which would result in lower fusion power. The influence of injecting high-atomic-number impurity for enhancing the core radiation in reactor plasma with internal transport barrier was studied in [3]. Influence of Ar and krypton injection into DEMO plasma was discussed based on the experiment in ASDEX Upgrade in [4]. In contrast, improvement of the core and pedestal confinement was reported in Ar-seeded H-mode plasmas in JT-60U [5], which would mitigate the degradation of the performance. Although the operation density would be reduced for the peaked density profile, the impurity accumulation in the core plasma would be enhanced, compared to the broad density profile. It is needed to increase the operation density to achieve the same fusion power under these conditions. Consequently, the peaked density profile may have higher operation density compared to the broad density profile, with Ar impurity injection.

In this Letter, we report on dependence of operation density and of seeded impurity accumulation on the density profile shape in DEMO plasmas using the integrated transport code TOTAL (Toroidal Transport Analysis Linkage) [6]. The simulation studies with impurity injection for ITER or DEMO plasmas were already reported [3, 7–11]. No radial transport of impurity ions was considered in [7–9]. In [10], the effects of the impurity pinch veloc-

author's e-mail: fujita@energy.nagoya-u.ac.jp

Table 1 The typical plasma parameters referred to [1, 9].

Parameter		Value
Plasma major radius [m]	R_P	8.50
Plasma minor radius [m]	a_P	2.42
Elongation	κ_{95}	1.65
Triangularity	δ_{95}	0.33
Toroidal magnetic field [T]	B_T	5.94
Total plasma current [MA]	I_P	12.3
Fusion power [MW]	P_{fus}	1462
α heating power [MW]	P_α	291
RF heating power [MW]	P_{RF}	83.7
Volume-averaged electron density $[10^{20}\ m^{-3}]$	$\langle n_e \rangle$	0.66
H factor (98y2)	HH_{98y2}	1.31
Normalized β	β_N	3.4

ity were studied for the fixed electron particle transport. Pacher *et al.* [11] examined the effect of the different impurity injection (i.e. neon, Ar, iron, and xenon) for DEMO plasma. However, only two cases with different inward velocities were investigated. Impurity ion transport with a systematic scan of the electron density profile seems to be reported in our work for the first time.

The plasma parameters in this study are based on those used in steady-state operation of JA DEMO 2014 [1, 9] and shown in Table 1. Dependence of the fusion power P_{fus} and the power through the separatrix P_{sep} on the concentration of Ar was studied using a system code in [9], without analysis of radial transport. In this study, one dimensional heat and particle transport was analyzed with a fixed safety factor profile with positive shear. In TOTAL, P_{fus} is calculated by integrating the local fusion power density determined by deuterium and tritium ion densities and the ion temperature. During the simulation, P_{fus} was fixed by the feedback control of the injection frequency of deuterium-tritium pellets. The cylindrical pellets (3 mm radius, 4 mm height) were injected from the high field side, at the speed of 1 km/s. The neutral gas shielding model was used for pellet ablation and the mass relocation model was used to consider the $\boldsymbol{E} \times \boldsymbol{B}$ drift of ablated materials [12]. The thermal diffusivity for ions and electrons, and the particle diffusivity for deuterium (D), tritium (T) and helium (He) ions by anomalous transport are given based on the mixed Bohm/gyro-Bohm model [13]. The H-mode pedestal was formed in the edge region $0.95 \le \rho \le 1$, where ρ is the normalized minor radius ($\rho = r/a_P$), by reducing the particle and thermal diffusivity using constant coefficients; here r is the effective minor radius and a_P is the effective plasma minor radius. The thermal diffusivity in the whole region was adjusted by another constant coefficient to have the H-factor relevant to the design value in [1, 9].

The particle flux Γ_k was given by the follows:

$$\Gamma_k = \Gamma_k^{NC} - D_k^{AN}\langle|\nabla r|^2\rangle(\partial n_k/\partial r) + V_k^{AN}\langle|\nabla r|\rangle n_k, \quad (1)$$

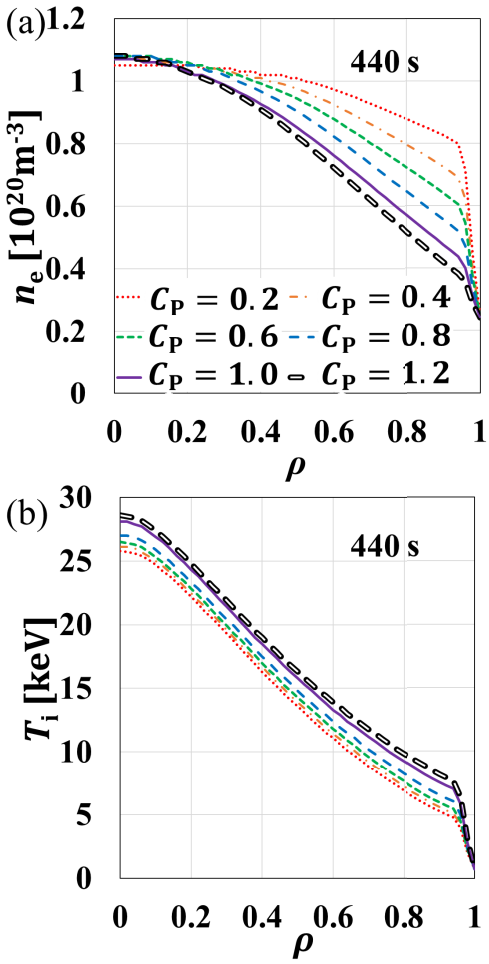

Fig. 1 The steady state (a) $n_e(\rho)$ and (b) $T_i(\rho)$ before Ar injection (t = 440 s).

$$V_k^{AN}\langle|\nabla r|\rangle = -C_P D_k^{AN}\langle|\nabla r|^2\rangle(2r/a_P^2), \quad (2)$$

where k denotes ion species including impurity ions, Γ_k^{NC} is the particle flux by neoclassical transport, D_k^{AN} and V_k^{AN} are the diffusivity and the pinch velocity by anomalous transport, n_k is the density, and $\langle|\nabla r|^2\rangle$ and $\langle|\nabla r|\rangle$ are metrics of the geometric factors, respectively. The C_P is a dimensionless coefficient for varying the anomalous pinch velocity and then the electron density profile. Γ_k^{NC} was calculated by the NCLASS module [14] included in TOTAL. For simplicity, D_k^{AN} for Ar ions was assumed to be twice larger than the diffusion coefficent by neoclassical transport for Ar ions, while D_k^{AN} for D, T and He ions was calcluated by using the mixed Bohm /gyro-Bohm model as mentioned above. V_k^{AN} was included only for D, T, and He, but not for Ar in order to examine the dependence of operation density and of seeded Ar accumulation on $n_e(\rho)$ shape. The recycling was considered for D, T, and He, but not for Ar.

The RF wave was employed for external heating and its power was linearly increased from 0 MW to 83.7 MW from start of the simulation (t = 0 s) to t = 80 s, and was kept constant after t = 80 s. A fixed radial profile

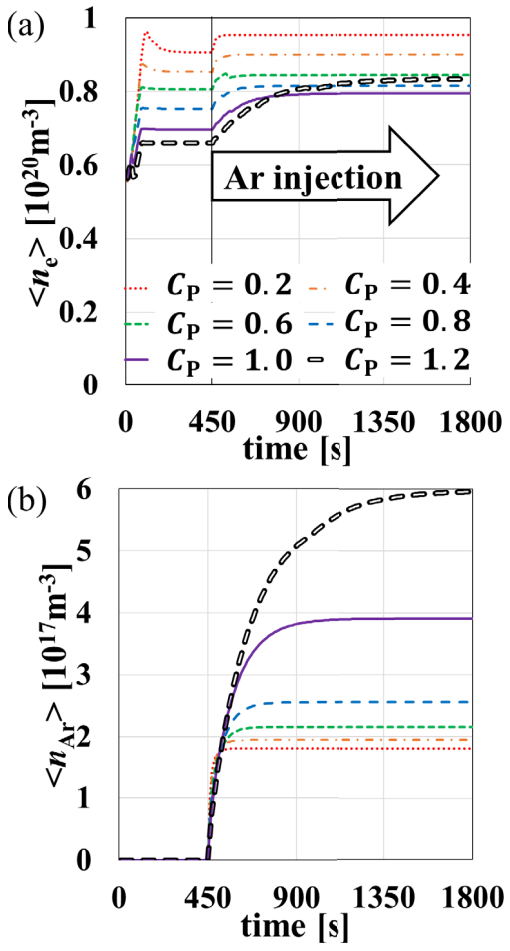

Fig. 2 The time evolution of (a) $\langle n_e \rangle$ and (b) $\langle n_{Ar} \rangle$. Ar was injected from 450 second.

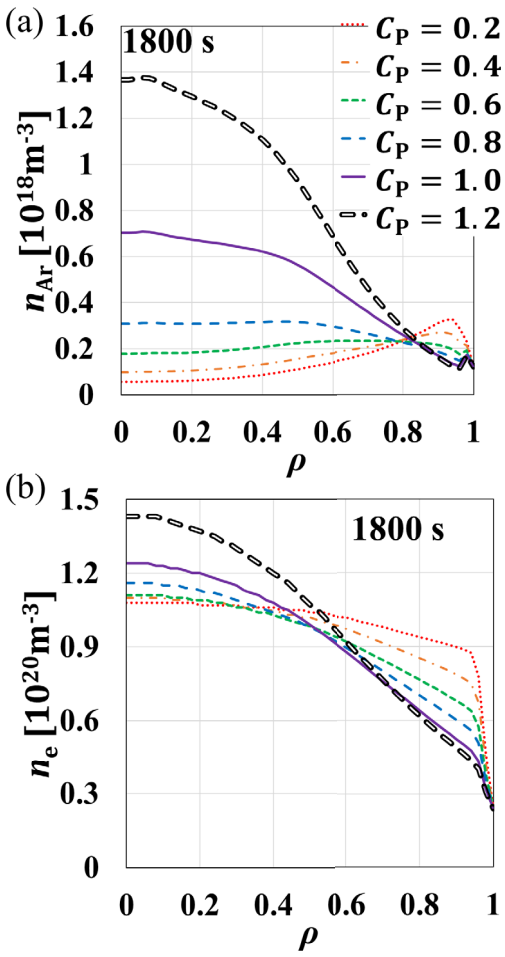

Fig. 3 The steady state (a) $n_{Ar}(\rho)$ and (b) $n_e(\rho)$ after Ar injection (t = 1800 s).

shape was assumed for RF power absorption. The command value of the α heating power P_α was also linearly increased 0 MW to 291 MW from t = 0 s to t = 80 s, and was kept constant after t = 80 s to achieve the target value of $P_{fus} = 5P_\alpha$, 1462 MW.

We scanned C_P, in the range between $0.1 \le C_P \le 1.2$, to vary the electron density profile $n_e(\rho)$. Ar was injected from t = 450 s. Referring to the divertor simulation of JA DEMO [9], we fixed boundary conditions of the ion temperature T_i, the electron temperature T_e, n_e, and the concentration of Ar; $T_i(1)$ = 740 eV, $T_e(1)$ = 350 eV, $n_e(1) = 2.4\times10^{19}$ m^{-3}, $n_{Ar}(1)/n_e(1) \approx 0.5\%$. The Ar injection rate was adjusted to fix $n_{Ar}(1)/n_e(1) \approx 0.5\%$, for each C_P, and it was approximately 4×10^{19} s^{-1}.

$n_e(\rho)$ and the ion temperature profile $T_i(\rho)$ in the steady state before Ar injection are shown in Fig. 1. Interestingly, $n_e(0)$ was almost constant regardless of the shape (the peakedness or the broadness) of $n_e(\rho)$. In the peaked $n_e(\rho)$ (higher C_P) cases, the pedestal density $n_e^{ped} = n_e(0.95)$ was lower and the pedestal temperature was higher than in the broad $n_e(\rho)$ (lower C_P) cases. In the whole region of the plasma, T_i was higher and n_e was lower in the peaked $n_e(\rho)$ (higher C_P) cases than in the broad $n_e(\rho)$ (lower C_P) cases, which resulted in the same P_{fus}. As shown in Fig. 1 (a), the same P_{fus} was obtained with lower volume-averaged electron density $\langle n_e \rangle$ in the peaked $n_e(\rho)$ cases.

The time evolution of $\langle n_e \rangle$ and that of the volume-averaged Ar density $\langle n_{Ar} \rangle$ are shown in Fig. 2. As shown in Fig. 2 (a), $\langle n_e \rangle$ before Ar injection was larger for broader $n_e(\rho)$. $\langle n_e \rangle$ increased after Ar injection. This was mainly due to the electrons released from the injected Ar. Increment of $\langle n_e \rangle$ and the accumulation of Ar ($\langle n_{Ar} \rangle$) was larger for more peaked $n_e(\rho)$ cases. The $\langle n_e \rangle$ was, however, the largest for the broadest $n_e(\rho)$ (C_P = 0.2) case even after Ar injection. It took a longer period to reach the steady state in the peaked $n_e(\rho)$ cases, compared the broad $n_e(\rho)$ cases.

The Ar ion density profile $n_{Ar}(\rho)$ and $n_e(\rho)$ in the steady state after Ar injection are shown in Fig. 3. $n_{Ar}(\rho)$ was hollow for low values of C_P ($C_P \le 0.4$), was nearly flat for C_P = 0.6, and was peaked for high values of C_P ($C_P \ge 0.8$). The Ar ions were fully stripped (Ar^{18+}) in almost the whole region expect for the periphery region (in the pedestal). $n_e(\rho)$ was affected by Ar injection.

Dependence of $\langle n_e \rangle$ and $\langle n_{Ar} \rangle$ on the density peaking factor $n_e(0)/\langle n_e \rangle$ is shown in Fig. 4 (a). $\langle n_e \rangle$(440 s)

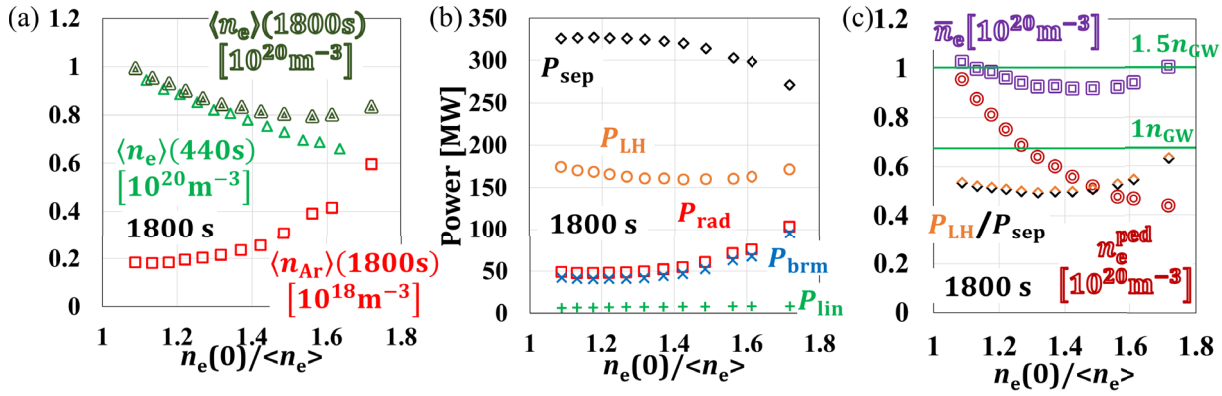

Fig. 4 The $n_e(0)/\langle n_e\rangle$ dependence of (a) $\langle n_e\rangle$ in the steady state before and after Ar injection (at 440 s and 1800 s, respectively), $\langle n_{Ar}\rangle$ at 1800 s in the steady state, (b) the powers (P_{sep}, P_{LH}, P_{rad}, P_{brm}, and P_{lin}) at 1800 s in the steady state, and (c) $\bar{n}_e$, n_e^{ped} and P_{LH}/P_{sep} at 1800 s in the steady state. n_{GW} is 0.67×10^{20} m^{-3} in this study.

decreased nearly linearly with $n_e(0)/\langle n_e\rangle$. On the other hand, $\langle n_{Ar}\rangle$ and then the increment of $\langle n_e\rangle$ due to Ar injection increased with $n_e(0)/\langle n_e\rangle$ and its dependence was stronger than linear. As a result, $\langle n_e\rangle$(1800 s) had the minimum around $n_e(0)/\langle n_e\rangle \sim 1.6$. Figure 4 (b) shows P_{sep}, the threshold power for L-mode to H-mode transition P_{LH}, the radiation power P_{rad}, the bremsstrahlung radiation power P_{brm}, and the line radiation power P_{lin} at 1800 s as functions of $n_e(0)/\langle n_e\rangle$. Here the formula given in Eq. (3) of [15] was used to evaluate P_{LH}. It was around 160 - 170 MW in this study. The synchrotron radiation was neglected and then $P_{rad} = P_{brm} + P_{lin}$. P_{lin} was small for all cases because Ar ions were fully stripped in almost the whole region. P_{rad} was then dominated by P_{brm}. P_{rad} and P_{brm} increased generally monotonically with $n_e(0)/\langle n_e\rangle$ while P_{sep} decreased generally monotonically with $n_e(0)/\langle n_e\rangle$. The line-averaged electron density $\bar{n}_e$, n_e^{ped} and P_{LH}/P_{sep} at 1800 s are shown as functions of $n_e(0)/\langle n_e\rangle$ in Fig. 4 (c). n_e^{ped} decreased monotonically with $n_e(0)/\langle n_e\rangle$ while $\bar{n}_e$ had the minimum around $n_e(0)/\langle n_e\rangle \sim 1.4$. $\bar{n}_e$ was around 1.5 times the Greenwald density n_{GW}. $n_e^{ped} < n_{GW}$ was obtained in $n_e(0)/\langle n_e\rangle > 1.3$. P_{LH}/P_{sep} was smaller than 0.65 in this study.

To maintain H-mode with good confinement, P_{sep} should be larger than P_{LH}. In this study, $P_{sep} > P_{LH}$ at 1800 s as shown in Figs. 4 (b) and (c). Therefore P_{rad} was not so large to degrade the energy confinement. $\bar{n}_e = 1.5n_{GW}$ (ASDEX) and $\bar{n}_e = 2n_{GW}$ (TFTR) were obtained while $n_e^{ped} \geq n_{GW}$ was not obtained in the experiment [16]. Considering these experimental results, the values of $\bar{n}_e$ and n_e^{ped} around $n_e(0)/\langle n_e\rangle \sim 1.6$ are considered feasible. Since $n_e(0.2)/\langle n_e\rangle \approx 2.0$ was obtained in the experiment [17], the range of $n_e(0)/\langle n_e\rangle$ in this study seems also to be feasible.

In conclusion, it was revealed that making peaked $n_e(\rho)$ can improve the feasibility of the DEMO operation density ($2n_{GW} > \bar{n}_e \approx 1.5n_{GW}$, $n_e^{ped} < n_{GW}$) under the fixed P_{fus} (pellet fueling) and Ar injection (heat load reduction). H-mode would also be sustained ($P_{sep} > P_{LH}$). It should be noted that the optimum value of $n_e(0)/\langle n_e\rangle$ would depend on the assumptions made in this analysis including $n_{Ar}(1)/n_e(1)$, the diffusion coefficient of Ar ions and the density gradient in the pedestal that further depends on the separatrix density and pedestal pressure. The anomalous pinch velocity was not considered for Ar in this study. Dependence on these parameters will be studied in future. It is also needed to include intrinsic impurities such as tungsten in the simulation. Furthermore, in this study, transport in the SOL and divertor plasmas were not analyzed and then the heat load of the divertor were not evaluated. We will introduce the radiation power model in the SOL and the divertor region to the TOTAL code in order to evaluate the heat load on the divertor target.

This study was performed with the support of the Collaboration Research Programme of Joint Special Design Team for Fusion DEMO in Japan.

[1] Y. Sakamoto *et al.*, FIP/3-4Rb, 25th IAEA FEC, St. Petersburg (2014).
[2] C. Angioni *et al.*, Plasma Phys. Control. Fusion **51**, 124017 (2009).
[3] T. Yamakami *et al.*, Plasma Fusion Res. **9**, 3403091 (2014).
[4] A. Kallenbach *et al.*, Plasma Phys. Control. Fusion **55**, 124041 (2013).
[5] H. Urano *et al.*, Nucl. Fusion **55**, 033010 (2015).
[6] K. Yamazaki *et al.*, Nucl. Fusion **32**, 633 (1992).
[7] T. Putterich *et al.*, Nucl. Fusion **59**, 056013 (2019).
[8] C.E. Kessel *et al.*, Nucl. Fusion **55**, 063038 (2015).
[9] N. Asakura *et al.*, Nucl. Fusion **57**, 126050 (2017).
[10] G. Giruzzi *et al.*, Nucl. Fusion **55**, 073002 (2015).
[11] G.W. Pacher *et al.*, Nucl. Fusion **47**, 469 (2007).
[12] T. Yamakami *et al.*, Plasma Fusion Res. **8**, 2403079 (2013).
[13] M. Erba *et al.*, Plasma Phys. Control. Fusion **39**, 261 (1997).
[14] W.A. Houlberg *et al.*, Phys. Plasmas **4**, 3230 (1997).
[15] Y.R. Martin *et al.*, J. Phys.: Conf. Ser. **123**, 012033 (2008).
[16] M. Greenwald, Plasma Phys. Control. Fusion **44**, R27 (2002).
[17] C. Angioni *et al.*, Nucl. Fusion **47**, 1326 (2007).